Fringe Field Maps for Cartesian Dipoles with Longitudinal and/or Transverse Gradients

Ryan Lindberg and Michael Borland

Argonne National Laboratory, 9700 S. Cass Avenue, Argonne, IL 60559

Argonne NATIONAL LABORATORY

NAPAC 2022

U.S. DEPARTMENT OF ENERGY

Argonne National Laboratory is a U.S. Department of Energy laboratory managed by U Chicago Argonne, LLC.

TUPA28

Abstract

Fringe field effects in dipoles can give rise to important linear and nonlinear contributions. This paper describes how to extend the classic results of Brown[1] and the more recent calculations of Hwang and Lee[2] to Cartesian dipoles with transverse and/or longitudinal gradients. We do this by 1) introducing a more general definition of the fringe field that can be applied to longitudinal gradient dipoles, 2) allowing for quadrupole and/or sextupole content in the magnet body, and 3) showing how to employ the resulting fringe maps as a symplectic transformation of the coordinates. We compare our calculation results with tracking for longitudinal and transverse gradient dipoles planned for APS-U.

1. FRINGE FIELDS FOR CARTESIAN DIPOLES

Cartesian dipoles have straight magnetic poles parallel to the z-axis.

- Entrance plane at angle θ.
- Hard edge along x.
- Propagation direction is z.
- Multipole components are defined in xyz coordinates.
- Fringe field is defined by the transition between 2 regions of nearly constant but distinct multipole content.

The dimensionless magnetic vector potential $\boldsymbol{a} = e\boldsymbol{A}/p_0$ can be written in a gauge with vertical componennt $A_y = 0$ as

$$A_z = \frac{x}{\rho}D(z) + \frac{x^3 - 3xy^2}{6\rho B_0}\frac{\partial^2 B_y}{\partial x^2} + \frac{x^2 - y^2}{2}KQ(z) - \frac{x^4 - 6x^2y^2 - y^4}{48}KQ''(z)$$

$$A_x = \frac{y^2}{2\rho}D'(z) - \frac{8y^4}{192\rho}D'''(z) + \frac{6x^2y^2 - y^4}{24\rho B_0}\frac{\partial^2 B'_y}{\partial x^2} + \frac{xy^2}{2}KQ'(z).$$

The dimensionless, on-axis dipole and quadrupole field profiles are related to the generalized gradient representation[3] via

$$D(z) = \frac{q\rho}{p_0}C_1(z) \qquad Q(z) = \frac{2q}{Kp_0}C_2(z),$$

while the field curvature term

$$\frac{1}{\rho B_0}\frac{\partial^2 B_y}{\partial x^2} = -\frac{q}{p_0}\left[\frac{1}{4}C_1''(z) - 6C_3(z)\right].$$

- The hard edge model uses step functions to match the integrated bending field.
- The hard edge location z_{edge} is set by

$$\int_{z_-}^{z_+} dz\ B_y(0,0,z) = \int_{z_-}^{z_+} dz\ C_1(z) = (z_+ - z_{\text{edge}})\Pi_1(z_+) + (z_{\text{edge}} - z_-)\Pi_1(z_-),$$
$$\Pi_1 = C_1(z_+)\Theta(z - z_{\text{edge}}) + C_1(z_-)\Theta(z_{\text{edge}} - z).$$

- The difference between the actual on-axis B_y and the hard edge model defines the dipole fringe field.
- Hard edge models for quadrupole and sextupole components are defined by z_{edge} and their maxima/minima at $z_\pm$.

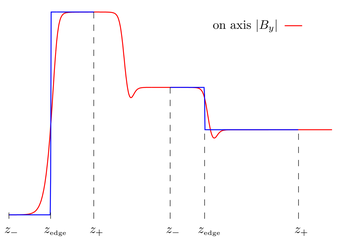

Figure 1: *On the left is the on-axis field profile (red) and hard edge model (blue) at the entrance edge where B_y starts from zero at z_- and reaches a maximum at z_+. On the right the difference between the red and blue shows the more complicated fringe in a longitudinal gradient dipole.*

2. DYNAMICS ON THE FRINGE

Motion in the fringe is governed by the expanded, dimensionless Hamiltonian

$$\mathcal{H}(\boldsymbol{x},\boldsymbol{p},\delta;z) \approx \frac{(p_x + a_x)^2\sec^3\theta}{2(1+\delta)} + \frac{p_y^2\sec\theta}{2(1+\delta)} - \delta + \delta\cos\theta + (p_x + a_x)\tan\theta + a_z.$$

Fringe field corrections are defined by the difference of $\mathcal{H}$ and the hard edge

$$\mathcal{H}_0 = \frac{\sec^3\theta}{2(1+\delta)}p_x^2 + \frac{\sec\theta}{2(1+\delta)}p_y^2 - \delta + \delta\cos\theta + p_x\tan\theta + x\frac{q}{p_0}\Pi_1(z) + (x^2 - y^2)\frac{q}{p_0}\Pi_2(z) + (x^3 - 3xy^2)\frac{q}{p_0}\Pi_3(z).$$

Our perturbation theory proceeds as

1. Define $\mathscr{B}_0(z|z_-)$ to be the unperturbed map associated $\mathcal{H}_0$ from $z_- \to z$.
2. The map $\mathscr{M}$ for $\mathcal{H}_0 + \mathcal{H}_1$ can be written using the "reverse factorization" [4]:

   $$\mathscr{M} = \mathscr{B}_1(z|z_-)\mathscr{B}_0(z|z_-),$$

   where $\mathscr{B}_1$ accounts for $\mathcal{H}_1$ such that

   $$-\frac{d}{dz}\mathscr{B}_1 = \mathscr{B}_1\left(\mathscr{B}_0 :\mathcal{H}_1: \mathscr{B}_0^{-1}\right) = \mathscr{B}_1 :\mathcal{H}_1^{\text{int.}}:.$$

3. The fringe field map $\mathscr{F}$ obtains by sandwiching the full dipole field map $\mathscr{M}$ between unperturbed dipole maps $\mathscr{B}_0$ to and from the edge:

   $$\mathscr{F} = \mathscr{B}_0(z_-|0)\mathscr{M}\mathscr{B}_0(0|z_+) = \mathscr{B}_0(z_-|0)\mathscr{B}_1(z_+|z_-)\mathscr{B}_0(0|z_-).$$

4. The fringe field map at the hard edge can then be written using the Magnus operator $\mathscr{F} = e^{:\Omega_M:}$ with Lie generator

   $$\Omega_M = -\int_{z_-}^{z_+} dz\ \mathcal{H}_1^{\text{int}}(z|0) + \frac{1}{2}\int_{z_-}^{z_+} dz \int_{z_-}^{z} d\zeta\ :\mathcal{H}_1^{\text{int}}(\zeta|0):\mathcal{H}_1^{\text{int}}(z|0) + \ldots$$

5. The fringe field correction at the hard edge for, e.g., the vertical coordinate, is then $\Delta y = (e^{:\Omega_M:} - 1)y_0$.

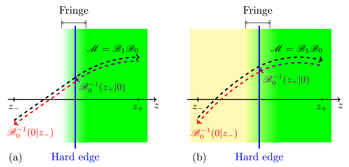

Figure 2: *Schematic of the fringe field map composite parts including the map to outside the fringe region (in red), through the fringe field (black), and back to the hard edge (violet). Panel (a) depicts the map for a dipole entrance, while (b) shows the case where the bending field transitions between two non-zero regions distinguished by yellow and green coloring.*

The resulting fringe field maps include hard edge generalizations of [1] such as

$$\Delta x = \frac{\sec^3\theta}{2(1+\delta)}\frac{y_0^2}{\rho} \to \frac{\sec^3\theta}{2(1+\delta)}\left[\frac{y_0^2}{\rho_+} - \frac{y_0^2}{\rho_-}\right] \quad (1)$$

$$\Delta p_y = -\frac{y_0}{\rho}\left[\tan\theta + \frac{\sec^3\theta}{1+\delta}p_{x,0}\right] \to \left[\frac{y_0}{\rho_-} - \frac{y_0}{\rho_+}\right]\left[\tan\theta + \frac{\sec^3\theta}{1+\delta}p_{x,0}\right] \quad (2)$$

and new quadrupole corrections including

$$\Delta x|_{\text{new}} = \frac{1 - \frac{3}{2}\tan^2\theta}{\cos^3\theta(1+\delta)}(g^2KI_1)x_0 \quad (3)$$

$$\Delta y|_{\text{new}} = -\frac{\sec\theta}{1+\delta}(g^2KI_1)y_0 \quad (4)$$

$$\Delta p_x|_{\text{new}} = -\frac{(1 - \frac{3}{2}\tan^2\theta)}{\cos^3\theta(1+\delta)}(g^2KI_1)p_{x,0} - \frac{\tan\theta}{4}(K_+ - K_-)(x_0^2 + y_0^2) \quad (5)$$

$$\Delta p_y|_{\text{new}} = \frac{\sec\theta}{1+\delta}(g^2KI_1)p_{y,0} - \frac{\tan\theta}{2}(K_+ - K_-)x_0y_0 \quad (6)$$

where the qudrupole fringe field integral

$$I_1 = \frac{2q}{g^2Kp_0}\int_{z_-}^{z_+} dz\ (z - z_{\text{edge}}) \times \left\{C_2(z) - C_2(z_+)\Theta(z) - C_2(z_-)[1 - \Theta(z)]\right\}$$

3. COMPARISON WITH TRACKING

- We assume the on-axis variation follows the Enge function $1/(1 + e^{-z/g})$ [5].
- We model $\boldsymbol{B}$ using the exact, one-parameter solutions provided in Ref. [6].
- We use tracking to evaluate the fringe field map using the following four steps:

1. Initialize coordinates on the hard edge $z = z_{\text{edge}} = 0$.
2. Drift particles to $z = -10g$ where $\boldsymbol{B} \approx \boldsymbol{0}$.
3. Track particles through exact magnetic field to $z = 10g$ where $\boldsymbol{B} \approx$ constant.
4. Back-track the particles to $z = 0$ using the ideal $\boldsymbol{B} = (p_0/q)(1/\rho + Ky, Kx, 0)$.

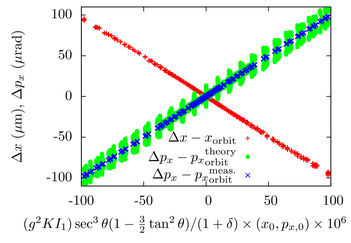

Figure 3: *Fringe Δx and Δp_x vs. initial x_0 and $p_{x,0}$ that are scaled such that Eqs. (3)-(4) predicts lines with slopes ∓ 1.*

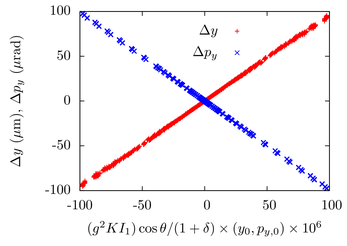

Figure 4: *Fringe Δy and Δp_y vs. initial y_0 and $p_{y,0}$ that are scaled such that Eqs. (5)-(6) predict the lines $y = \pm x$.*

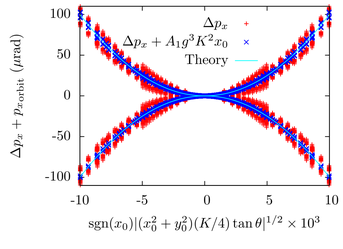

Figure 5: *Δp_x corrected by the theory's offset $p_{x\text{orbit}}$ (red), and by an empirically found focusing $\propto g^3K^2x_0$. The offset is scaled so Eq. (5) follows $y = \pm x^2$ (cyan).*

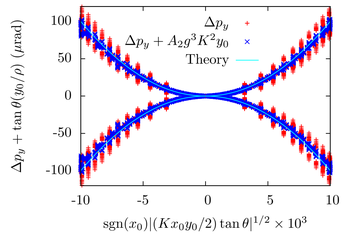

Figure 6: *Δp_y corrected by the theoretical focusing (red) and by an empirically found focusing $\propto g^3K^2y_0$ (blue). The offset product $|x_0y_0|^{1/2}$ is scaled such that Eq. (6) predicts the cyan parabolas $y = \pm x^2$.*

- APS-U's AM1 dipole uses 5 magnetic segments for its longitudinal gradient.
- This leads to 6 fringe field maps.

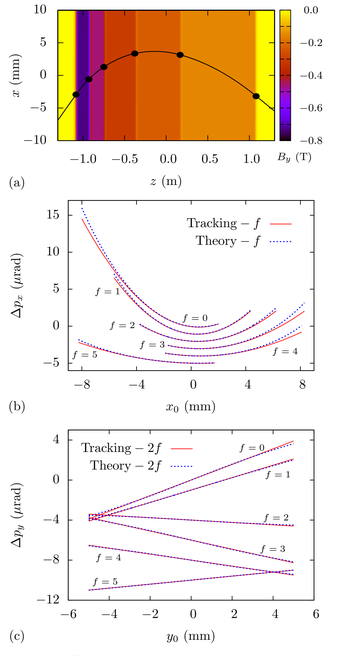

Figure 7: *(a) The AM1 longitudinal gradient dipole field profile and reference orbit. The hard edges of each magnetic segment are identified with black circles. (b) Comparison of tracking (red solid lines) with theory (blue dashed lines) for the fringe field corrections Δp_x as a function of input x_0 at each hard edge. The lines are displaced by the fringe number $0 \le f \le 5$ for clarity. (c) Analogous comparions of tracking and theory for the vertical focusing Δp_y at each edge.*

4. `elegant`[7] TRACKING

- We added the fringe field model to `elegant`'s `CCBEND` element [8].
- We have compared the resulting models against tracking in the full field.

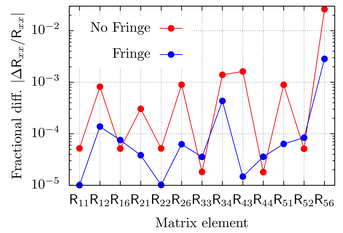

Figure 8: *`CCBEND`'s linear matrix element predictions for the APS-U Q4 transverse gradient dipole.*

The differences change the lattice tunes, in good agreement with generalized-gradient-expansion model (BGGEXP) [9]

Model	ν_x	ν_y
`BGGEXP`	94.9856	36.0878
`CCBEND`+Fringe	94.9832	36.0872
`CCBEND`+No Fringe	95.0038	36.1560

- Theory has also been added to the new `LGBEND` (longitudinal gradient bend) element.
- The fringe integrals for both `CCBEND` and `LGBEND` can be easily evaluated using the companion program `straightDipoleFringeCalc`.

Acknowledgments

Work supported by the U.S. Deptartment of Energy, Office of Science, Office of Basic Energy Sciences, under Contract No. DE-AC02-06CH11357.

References

[1] K. L. Brown. SLAC-R-75, SLAC (1982).

[2] K. Hwang, et al. *Phys Rev ST-Accel Beams*, 18:122401 (2015).

[3] M. Venturini. Ph.D. thesis, University of Maryland (1998).

[4] A. J. Dragt. Lie Methods for Nonlinear Dynamics with Applications to Accelerator Physics. University of Maryland (2009).

[5] H. A. Enge. *Rev Sci Instr*, 34:385 (1963).

[6] B. D. Muratori, et al. *Phys Rev Accel Beams*, 18:064001 (2015).

[7] M. Borland. ANL/APS LS-287, Advanced Photon Source (2000).

[8] M. Borland. LS-356, Advanced Photon Source (2021).

[9] M. Borland et al. These proceedings, MOPAB059.